Improving stability of biosensor based on covalent immobilization of horseradish peroxidase by γ-aminobutyric acid and application in detection of H2O2

Mina Feizabadi, Ahmad Soleymanpour, Hassan Faridnouri, Davood Ajloo

PII: S0141-8130(19)32348-7
DOI: https://doi.org/10.1016/j.ijbiomac.2019.06.103
Reference: BIOMAC 12609

To appear in: *International Journal of Biological Macromolecules*

Received date: 31 March 2019
Revised date: 5 June 2019
Accepted date: 14 June 2019

Please cite this article as: M. Feizabadi, A. Soleymanpour, H. Faridnouri, et al., Improving stability of biosensor based on covalent immobilization of horseradish peroxidase by γ-aminobutyric acid and application in detection of H2O2, International Journal of Biological Macromolecules, https://doi.org/10.1016/j.ijbiomac.2019.06.103

Improving stability of biosensor based on covalent immobilization of horseradish peroxidase by γ-Aminobutyric acid and application in detection of H_2O_2

Mina Feizabadi[a], Ahmad Soleymanpour[a], Hassan Faridnouri[b], Davood Ajloo[a*]

[a]School of Chemistry, Damghan University, Damghan, 36715-364, Iran

[b]School of Biology, Damghan University, Damghan, 36715-364, Iran

* Corresponding author: ajloo@du.ac.ir

Abstract

A novel electrochemical biosensor for the determination of hydrogen peroxide (H_2O_2) has been fabricated through covalently immobilized horseradish peroxidase (HRP) on modified multi walled carbon nanotube (MWCNT) by γ-aminobutyric acid (GABA) on glassy carbon electrode. using the electrochemical techniques, the electrochemical properties of the biosensor were specified. Cyclic voltammograms of the enzyme film at pH=7.0 exhibited a pair of quasi-reversible redox peaks according to Fe(III/II) redox process of HRP. The biosensor exhibited good efficiency for finding H_2O_2 with a broad linear range from 2.0×10^{-7} M to 2.81×10^{-4} M and a detection limit of 0.13 μM. The surface coverage of active HRP, heterogeneous electron transfer rate constant and Michaelis-Menten constant of immobilized HRP were obtained 3.029×10^{-9} mol cm^{-2}, 1.11 s^{-1}, and 0.23 mM respectively. Similarly, the applicability of the suggested biosensor was examined by detecting H_2O_2 in human plasma samples and the average recovery was obtained as 100.50±0.25. Moreover, the constructed biosensor presented a high stability, reproducibility and repeatability. Finally using docking and the molecular dynamics calculations, it was determined that GABA interacts with lysine residue and it causes HRP to be placed on the electrode with a specific orientation.

Keywords: Horseradish peroxidase, Hydrogen peroxide, Carbon nanotube, γ-aminobutyric acid.

1. Introduction

Hydrogen peroxide is one of the important intermediates in enzymatic reactions and acts as a strong oxidant [1]. The quick and accurate detection of H_2O_2 is very important in food and medicine industries and environmental assays [2-5], since it plays a crucial role in many redox processes in biological systems and the surrounding environment [6]. Electrochemistry methods are among the bsest and useful methods for detecting and determining. They have wide range applications like ambient N_2 fixation to NH_3 [7], the hydrogen evolution reaction (HER) [8] and biosensors [9]. they have advantages such as low cost, easy use, reliability, high sensitivity and selectivity [10]. Therefore in recent years, the improvement of biosensors based on peroxidase-modified electrodes has been mostly used in electroanalytical chemistry [11].

On the other hand, among peroxidases, horseradish peroxidase (HRP) has been widely used to improve biosensors based on enzymes. HRP is an oxidoreductase which acts as an electron acceptor compound and catalyzes the reduction of hydrogen peroxide. HRP is inexpensive, available and acts specifically; therefore, it has been widely employed in biosensors for H_2O_2 determination [12]. But the active site of the enzyme is in a deep place and its accessibility is a major challenge for the direct electrochemistry of HRP. According to Marcus theory, the less distance and the desirable orientation increase the direct electron transfer [13]. Another challenge in working biosensors is the rapid loss of enzyme activity due to its interaction with the electrode surface and so enzyme unfolding. The typical lifetime of biosensors is only 2-4 weeks; however, by a good physicochemical environment to which the protein is exposed (e.g., supporting matrix) enzyme stability issues could be improved. This, in turn, changes the optimum pH, thermal stability, and therefore the kinetic parameters.

Various materials such as; nanoparticles [14-16], ionic liquids [17] and conducting polymers [18, 19] were used to suit the enzyme surrounding to accelerate electron transfer between the enzyme and the surface of the electrode. Additionally, several materials have been studied for the enhancement of DET and the current response between the electrode and the HRP enzyme such as; gold nanoparticles (AuNPs) [14], cadmium sulphide [CdS] nanofibers [20], and carbon nanomaterials [21]. In recent decades, due to the unique properties of carbon nanomaterials, such as fast electron transfer, high thermal conductivity, excellent mechanical flexibility and good biocompatibility,they have been used in a different fields such as electrochemical sensor and biosensor [22, 23] and supercapacitors [24]. These nanomaterials include graphene, graphene

oxide, carbon nanotube, and etc. Carbon nanotubes (CNTs) are one of the most important of these materials, which have received a great deal of attention. CNTs have unique mechanical, chemical and electronic properties and high volume ratio [25]. Recent investigations have shown that CNTs modified electrodes not only increase current at the electrode surface, but also have a great electrocatalytic activity towards some electroactive materials such as; caffeic acid [26], and glucose [27] and H_2O_2 [28]. There are also materials used by researchers to enhance the biosensor performance. For instance, Griebenow and his coworkers [9] have presented an effective method to immobilized HRP enzyme using the formation of a monolayer on the gold nanoparticle modified glassy carbon electrode. In addition, Wei Zhuang et al. [29] have expanded strategies to improve the activity and stability of immobilized glucose oxidase and catalase by attachment of the linear structured polymer of ε-Poly-L-lysine to enzyme.

By choosing a suitable matrix, controlled orientations of redox enzyme [9] and a good strategy to immobilize the enzyme such as entrapment [17], covalent binding [30] and etc., biosensor stability and sensitivity can be improved. It has been shown that the enzyme immobilization by a covalent bond prevents the enzyme from leaching the electrode surface and improves the efficiency of the biosensor. Several studies have been hitherto reported to improve biosensors of H_2O_2 based on covalent immobilization of HRP enzyme on modified electrode [31, 32].

In this study, a biosensor was fabricated based on covalent immobilization of HRP enzyme on modified functionalized multi walled carbon nanotube (MWCNT) by γ-aminobutyric acid (GABA) on glassy carbon electrode (GCE) surface for H_2O_2 concentration measurement. GABA is well-known as a neurotransmitter that adjusts inhibitory neurotransmission in mammalian central nervous systems [33]. Given that GABA is a chemical compound in living systems, particularly in the most sensitive part, the central nervous system, it therefore seems to have a suitable biocompatibility ; consequenly it can lead to increased stability and improved efficiency of the biosensor. On the other hand, GABA is a zwitterion with amine and carboxylic terminal which can act as a linker between enzyme and MWCNT through covalent couplings. Considering the possibility of compatibility of GABA in this study, an electrode modified with carbon nanotubes connected to GABA was used to the HRP immobilization and the optimum conditions and the performance parameters of the resulted biosensor were studied. Docking and

molecular dynamics studies confirmed and justified the obtained results from the experimental section..

2. Experimental

2.1. Materials and methods

Horseradish peroxidase (HRP, EC1.11.1.7, Type VI), Multi-walled carbon nanotube, N-(3-Dimethylaminopropyl)-N′-ethyl carbodiimide hydrochloride (EDC), N-hydroxysuccinimide (NHS) and γ-Aminobutyric acid were purchased from Sigma-Aldrich. Hydrogen peroxide (H_2O_2, 30% w/w), sulfuric acid and nitric acid were received from Merck and solutions were daily and freshly prepared. To prepare phosphate buffer solutions with different pH, standard stock solutions of 0.10 M Na_2HPO_4 and 0.10 M NaH_2PO_4 were mixed together and to adjust pH, 0.1 M HCl or NaOH were used from Merck. Water was purified by deionization and distillation.

2.2. Apparatus

The experiments were achieved by using a potentiostat/galvanostat (AUTOLAB PGSTAT-30) the GPES 4.9 and FRA 4.9 softwares were applied for voltammetric and electrochemical impedance spectroscopy (EIS), respectively (Eco-Chemie, Utrecht, Netherlands). A three-electrode system was employed with an Ag/AgCl (3 M KCl) as the reference electrode, a platinum wire as the counter electrode, and the modified glassy carbon electrode (GCE) as the working electrode. All experiments were done in a working solution (a 0.1 M phosphate buffer of pH=7.0) at 25 ±2 °C.

FT-IR spectra of the samples were recorded on a PERKIN ELMER RX I FT-IR spectrophotometer. EIS was carried out in the presence of 5.0 mM $K_3[Fe(CN)_6]/K_4[Fe(CN)_6]$ in 0.1 M KCl as a redox probe in the frequency range of 0.10 Hz–100 kHz, amplitude of 5.0 mV. The scanning electron microscopy (SEM) images of electrodes were characterized by using an MIRA3TESCAN-XMU field-emission SEM. Both samples were sputter-coated by platinum before SEM observation.

2.3. Procedures

2.3.1. Carboxylation of MWCNTs

First, Pristine MWCNTs are heated at 400° C for 2 h to burn off the pollution of their amorphous carbon. Then, 3 mg of purified MWCNT was dispersed in a test tube containing 8 mL mixture of concentrated sulfuric acid and nitric acid (3:1, v/v) in order to introduce carboxyl groups on their surface. The slurry was placed under the bath of ultrasonic waves (160HT, Soniclean Pty Ltd,

Seoul, Korea) for 3 h. Afterwards the product was centrifuged three times without any interruptions for 10 min at 3000 rpm and the pellet was rinsed with 5 mL of 0.1 M PBS (pH=7.0) between each centrifugation. The product is MWCNT-COOH.

2.3.2. Activation of MWCNT-COOH

3 mg of MWCNT-COOH was added to 1 ml of PBS (0.1 M, pH=7.0) containing EDC 400 mM and NHS 100 mM and the mixture was stirred at 250 rpm for 90 min. Then, it was centrifuged for 8 min at 4000 rpm and rinsed with PBS to remove the excess of EDC and NHS. Finally, it was dried in a vacuum oven. The carboxyl groups of MWCNT-COOH were converted to the active ester (succinimidyl ester) using NHS in the presence of the coupling agent EDC. Then, the product was added to 1.0 ml of GABA solution (1M) and stirred at 250 rpm for 12 h to form an amide bond between the activated carboxyl group of MWCNT-COOH and amine terminated of GABA (Fig. 1). Then the same above mentioned steps were also performed to activate the carboxylic terminated of GABA. The Product is MWCNT-COOH-GABA.

Fig.1

2.3.3. The working electrode preparation

Prior to modification, GCE was mechanically polished with 0.5 μm alumina powder slurries to a mirror-like surface and was rinsed ultrasonically with a mixture of acetone and HNO_3 (0.1 M) 1:1 (v/v), then washed with NaOH (1.0 M) and ultrapure water respectively for 3 min. Typically, 8.0 μl of the dispersion containing MWCNT-COOH-GABA in PBS (0.1 M. pH=7.0) was dropped onto the cleaned GCE and was allowed to dry under ambient conditions for 1h (MWCNT-COOH-GABA/GCE). Then, the electrode was immersed in a 5 mg ml^{-1} HRP solution in 0.1 M PBS at pH=7.0 for 24 h at 4°C. The electrode (HRP/MWCNT-COOH-GABA/GCE) was again rinsed with distilled water, dried and kept in the refrigerator.

Fig. 2

2.4. Model and computational method

Molecular docking study was performed in order to find out the binding sites on HRP. Geometry optimization of GABA (Fig. 3) was accomplished by Gaussian 03 program [34] with B3LYP

type exchange correlation functional and 6-311++G(d,p) basis set. The crystal structure of HRP with PDB ID 1H5A was obtained from Protein Data Bank (http://www.rcsb.org). The ligands and water molecules were removed, and then hydrogen atoms were added to the enzyme structure. The docking experiments were performed by Autodock 4.6 docking software using a genetic algorithm [35]. For the identification of the binding sites in HRP, docking was performed by using a box size of 126- 126-126 Å with grid resolution of 0.71 Å. The docking runs were performed on the Autodock engine with a maximum of 200 candidate poses and GABA was selected as flexible. The conformations were ranked by using the Ascore scoring function, which estimates the free binding energy. After the molecular docking, bonding sites of HRP-GABA were further analyzed by using DS Visualizer 2.0.

Fig. 3

Simulations of molecular dynamics were investigated in two modes: in the absence and in the presence of GABA. Gromos96 force field and spc model water was applied for calculations. A twin range cutoff was used for longer-range interactions; 1.0 nm for van der Waals interactions and 1.0 nm for electrostatic interactions. The particle mesh Ewald (PME) [36] method was used for calculating long-range interaction. A cubic simulation box of the volume 350.76 nm^3 was made and 5 molecules of GABA were randomly placed in this box. Then, 10111 molecules of water were randomly added into the simulation box. The initial configurations were minimized by using the steepest descent algorithm [37] with 10000 integration steps and the system was equilibrated for 30 ns at constant pressure (1.0 atm) and temperature (300 K) using the Parrinello–Rahman procedure. By using the GROMACS 5.1.1 package, all MD simulations were carried out.

3. Results and discussion

3.1. Infrared characterization

FT-IR was used to confirm the functionalization of MWCNT with the carboxylic group and then covalent attachment of GABA. Fig. 4 shows the FT-IR spectra of pristine MWCNTs, MWCNT-COOHs and MWCNT-COOH-GABA (a-c). The peak at 1648 cm^{-1} is related to the C=C stretching, which demonstrates the graphite structure of MWCNTs. A new appeared peak around 1700 cm^{-1} in the spectra of MWCNT-COOHs is assigned to C=O stretching of the carboxylic

acid group [8, 21]. Peaks of C–O and OH stretching vibrations of the carboxylic acid group can be seen at 1024 and 3429 cm^{-1} respectively [21]. With regard to the FT-IR spectra, it can be concluded that MWCNT has been successfully modified and carboxyl groups are located onto it. In Fig.4c, the appearance of a peak in 1760 cm^{-1} is devoted to the stretching of C-O. In addition, the presence of the new peak in 1223 cm^{-1} is related to the C-N bond and indicates the presence of the amide functional group. The peak at 3400 cm^{-1} indicates the presence of the O-H band in the GABA molecule, which is located on the carbon nanotube surface.

Fig. 4

3.2. Surface morphological characterizations using SEM

Surface morphology of the enzyme electrode was examined by scanning electron microscopy. Fig. 5A and B show SEM images of MWCNT-COOH-GABA/GC and MWCNT-COOH-GABA/HRP/GC modified electrode respectively. It can be seen that MWCNT-COOH-GABA exist as bundles entangled with one another (Fig. 5A). Fig.5 vividly shows that the thickness of MWCNT-COOH-GABA was increased by the addition of HRP and the electrode surface was packed with the uniformly distributed dense enzyme. It can be concluded that the HRP has been successfully deposited onto MWCNT-COOH-GABA surface.

Fig. 5

3.3 Electrochemical impedance spectroscopy

EIS is a sensitive method that can provide useful information on the impedance changes of the electrode surface during the preparation process of biosensor. In impedance spectra, the semicircle diameter equals the electron transfer resistance (R_{et}) at the electrode surface. R_{et} describes the interface properties of the electrode. For impedance measurements, a frequency ranges of 0.10-100 kHz was employed. The AC voltage amplitude was 5 mV, and the equilibrium time was 10 min. Fig. 6 exhibits the impedance spectra of the bare GCE and modification electrodes including MWCNT-COOH-GABA/GCE and MWCNT-COOH-GABA/HRP/GCE in 5.0 mM $K_3[Fe(CN)_6]$/ $K_4[Fe(CN)_6]$ solution and 0.1 M KCl. It is clear that R_{et} was decreased with progress in the modification stages. The bare GCE has a relatively high resistance. But with the addition of MWCNT-COOH-GABA, the electrode's resistance was

significantly reduced, which was attributed to the good conductivity of MWCNT-COOH-GABA. However, the R_{et} of MWCNT-COOH-GABA/HRP increases, showing that the HRP was immobilized onto the surface electrode. Therefore, the results indicate that the modification of GCE by MWCNT-COOH-GABA causes the construction of an electrode with the least resistance that is an advantage to building a biosensor.

Fig. 6

3.4. Investigation of electrochemical behavior of various film modified GCE's using cyclic voltammetric studies

The electrochemical behavior of the bare GCE, MWCNT-COOH/GCE, MWCNT-COOH-GABA/GCE and MWCNT-COOH-GABA/HRP/GCE in 10.0 mL PBS 0.1 M (pH=7.0) at scan rate 100 mV s^{-1} electrode was studied by using cyclic voltammetry. As seen in Fig. 7, there is no voltammetric response at the cyclic voltammograms of the bare GCE, MWCNT-COOH/GCE and MWCNT-COOH-GABA/GCE in solution (Fig. 7 a,b and d), On the other hand, according to Fig. 7c, immobilization of HRP on the MWCNT-COOH/GCE has a slight reduction peak and does not have a quasi-reversible property. Meanwhile, peak has appeared in the negative potentials which increases the interference. Actually the direct binding of the enzyme to the carboxylic carbon nanotube causes the HRP flexibility to weaken and thus reduces its activity. So MWCNT-COOH alone does not provide a suitable environment for enzyme immobilization. while MWCNT-COOH-GABA/HRP on GC electrode indicated a pair of quasi-reversible at about −0.03 and +0.07 V vs. Ag/AgCl at scan rate of 100 mV/s (Fig. 7f). Therefore, in the presence of GABA, both anodic and cathodic peaks are observed and the cathodic peak is shifted to higher voltages. Meanwhile the presence of GABA as a linker has less effect on molecular flexibility. GABA has also a short chain, therefore causes the redox center of the enzyme is placed near to the electrode surface in a more appropriate orientation. The formal potential (E°′) of MWCNT-COOH-GABA/HRP /GCE is specified to be 50 mV vs. Ag/AgCl (249 mV vs. NHE), which is almost at the range of the E°′ values reported for HRP from various literatures and methods of immobilization. The ratio of the cathode to the anodic current is approximately close to unity.

Fig. 7

3.5. The effect of scan rate

Fig. 8 shows a pair of redox peaks for the direct electron transfer behavior of immobilized HRP at various scan rates. Increasing the potential scan rate, both the anodic and cathodic peak currents enhanced. The linear relationship between the current peaks and the scan rate (shown in the inset (A) of Fig. 8) represents a surface controlled reversible process, which is expected from an immobilized enzyme system. The regression equation was obtained: I_{pc} (μA) = 85.77 ν (V s^{-1}) -2.72, R^2 = 0.997; I_{pa} (μA) = –84.85 ν (V s^{-1}) +2.50, R^2 = 0.998.

With the enhancement of scan rate, the anodic peak potential shifted towards a more positive value and the cathodic peak potential shifted towards a more negative value. The peak-to-peak separation is 102 mV at a scan rate of 100 mV s^{-1}. The smaller E_{pa}/E_{pc} can be attributed to the fact that HRP molecules are probably immobilized in one orientation [38]. Based on the Laviron theory [39] for a reversible reduction reaction of an absorbed species to the electrode surface can be calculated the amount of electroactive HRP enzyme on the electrode surface, by using the slope of $I_{pc} \propto \nu$ curve (inset A of Fig. 8) and by placing in Eq. 1.

$$Ip = \frac{\nu n^2 F^2 A \Gamma}{4RT} \quad (1)$$

Where I_p is the value of peak reduction, Γ is the electroactive HRP amount (mol cm^{-2}), n is the number of electrons transferred, F is the Faraday constant (96485 C mol^{-1}), A is the surface area of the electrode (cm^2), ν is the scan rate (mV s^{-1}), R is the gas constant (8.314 J mol^{-1} K^{-1}), and T is the Kelvin temperature (K). Assuming a single electron reaction, the surface coverage of HRP on the surface of the modified electrode was calculated to be 3.029×10^{-9} mol cm^{-2} [40]. The slope of log I_{pc} vs. log ν (inset B of Fig. 8) was obtained to be 1.35, with correlation coefficient equal 0.99, which confirms that a thin layer is formed at the electrode surface.

Fig. 8

Furthermore, the relationship between redox peak potentials and scan rate was investigated, and the electron transfer kinetic of HRP was obtained by using the Laviron model [41]. The charge-transfer coefficient (α) was estimated as 0.48. The heterogeneous electron transfer rate constant (k_s) was calculated according to the following equation:

$$\log k_s = \alpha \log(1-\alpha) + (1-\alpha)\log\alpha - \log\frac{RT}{nF\vartheta} - \frac{\alpha(1-\alpha)nF\Delta E_p}{2.3RT} \quad (2)$$

According to Eq. 2, the electron transfer rate constant (k_s) was obtained 1.11 s^{-1} by using the data for 100 mV s^{-1} from Fig. 9 via a previous reported method [41]. From the k_s value, it can be concluded that in this study, covalently immobilization of HRP by MWCNT-COOH-GABA, enhanced the rate of electron transfer [42].

Fig. 9

3.6. The effect of pH

The effect of pH on the current response of the biosensor was evaluated in the range of 5.0 to 8.5 in 0.10 M PBS. As shown in Fig. 10, both the anodic (E_{pa}) and cathodic (E_{pc}) potential shifted to negative values with the enhancement of pH that means the protons influence on the redox process. Therefore, the pH of the environment is effective on the protonation/deprotonation of some of the amino acids in the active site. As a result, pH plays an important role both in the change of HRP active-site conformation and its catalytic power. Consequently, it is worth noting that proton transfer is occurred in the electrochemical process. As shown in the inset of Fig. 10, the slope of potential (E) vs. pH was −56 mV/pH for immobilized HRP, which is in agreement with the slope of Nernst equation (−59 mV/ pH) [43].

Fig. 10

3.7. Electrocatalytic properties of MWCNT-COOH-GABA/HRP/GCE

The electrocatalytic activity of MWCNT-COOH-GABA/HRP/GCE was investigated toward H_2O_2 by differential pulse voltammetry method. Fig. 11A indicates DPV curves for different concentrations of H_2O_2 in 0.1 M PBS (pH=7.0). The proportional anodic peak was obtained for concentrations of 0.2 to 400 μM for H_2O_2. The proposed biosensor showed a linear calibration range for H_2O_2 from 2.0×10^{-7} to 2.81×10^{-4} M, [I (μA) = 0.089C (μM) + 1.747, R^2 = 0.997] (Fig. 11B). The detection limit (signal/noise =3) of the suggested biosensor was obtained 0.13 μM for hydrogen peroxide. In the Table 1, the performance of this electrode is compared with other modified electrodes. The detection limit of the biosensor is lower than the detection limits of some electrodes modified with various materials [44].

Fig. 11

Using the apparent Michaelis–Menten constant (K_m^{app}), the kinetics of the enzyme-substrate for the biosensor can be shown and was calculated from the electrochemical model of the Lineweaver–Burk equation [45].

$$\frac{1}{I_{ss}} = \frac{K_m^{app}}{I_{max}C} + \frac{1}{I_{max}} \quad (3)$$

Where I_{ss} is the steady state current after the addition of substrate and I_{max} is the maximum current measured under saturated substrate condition. The K_m^{app} and I_{max} values of the biosensor were found to be 0.23 mM and 39.6 μA for H_2O_2 respectively, (inset of Fig. 12B). A lower K_m^{app} value indicates a greater tendency of H_2O_2 to the enzyme and the enzyme activity has increased in the stabilized state. As a result, it can be concluded that the immobilized HRP onto MWCNT-COOH-GABA preserves its enzymatic bioactivity and the proposed biosensor shows a high dependency for H_2O_2. Table 1 compares the analytical properties of the biosensor in this study with previously reported.

Table 1

3.8. Stability of the MWCNT-COOH-GABA/HRP/GCE

Reproducibility and stability are essential requirements for a biosensor. The reproducibility of the MWCNT-COOH-GABA/HRP/GCE biosensor was investigated at H_2O_2 concentration of 10 μM. Five successful measurements were taken and RSD was obtained from 1.29%, which indicated a good reproducibility of the MWCNT-COOH-GABA/HRP/GCE biosensor. Then the storage stability of the biosensor was investigated. According to Fig. 12A, no significant change (<1%) in the cyclic voltammetric responses was seen even after repeating 50 continuous scans between −0.5 V and 0.5 V at 100 mV s^{-1}. The long-term stability of this biosensor, which was kept at 4°C when not in use, shows that the electrode still yielded about 90% of the initial current response after ten weeks (Fig. 12B). In addition, the long-term stability of the biosensor was studied by measuring its response current to 80.0 μM H_2O_2 (Fig. 12C). The current of the biosensor is nearly unchanged during the first 7 days. The biosensor still retains 92.65% of its original current after three weeks of storage. The reason for the better biosensor stability can be

attributed to the covalent bond between the GABA molecules and the HRP enzyme amino acids which cause a good and stable immobilization at the electrode surface.

Fig. 12

3.9. Analysis of real samples

To measure the usability of the suggested biosensor for clinical potential applications as a real sample, the concentration of H_2O_2 in human plasma sample was determined under optimum conditions. The samples were diluted 100 times with PBS (pH=7.0) before analysis with no further pretreatments. Different amounts of H_2O_2 were then spiked into the plasma sample and the standard addition method was used to obtain the results. The analytical results are displayed in Table 2. Statistical t-test showed that there is an agreement between spiked and obtained results, which revealed that the proposed MWCNT-COOH-GABA/HRP/GC electrode can be applied in order to determine H_2O_2 concentration in real sample with satisfactory accuracy and precision.

Table 2

3.10. Computational results

Algorithms in the docking calculation make the ligand to move randomly around HRP in a box with a definite size so that the ligand scans different sites of macromolecules by using accompanying algorithm implemented in the Autodock. Past researches have shown that lysine amino acids on one side of the HRP have a better ability to modification [46]. Based on the docking results in Fig. 13, GABA mostly tend to bind to Lys-232, Lys241 and Lys 65. Ghourchian et al. obtained similar results in the modification of lysine aminoacids with anthraquinone 2-carboxylic acid [46].

Fig. 13

The conformational changes of the system during MD simulations were monitored by the root–mean–square derivations (RMSD). The results showed that RMSD of the HRP+GABA is less

than HRP (Fig. 14A) indicating that the enzyme's flexibility was reduced in the presence of GABA.

Moreover, the solvent accessible surface area (SASA) was calculated and the results showed that in the presence of GABA, more amino acids are available to the solvent (Fig. 14B). On the other hand, H_2O_2 has to diffuse from the surface of the enzyme to the heme prostatic group so that it can interact with heme group. According to studies, it has been determined that H_2O_2 passes through a channel along with the fluctuation of Phe-68 and Phe-142 and reaches the heme iron. Phe-68 and Phe-142 are at the channel entrance, and their conformational fluctuations determine the accessibility of H_2O_2 to the interior. MD results demonstrates that with the presence of GABA, the average distance between the backbones of Phe-68 and Phe-142 increases from 10.40 and 11.45 Å (Fig. 15A), to 11.43 and 13.62 Å (Fig. 15B), respectively. Therefore, it can be said that in the presence of GABA the channel entry has been expanded and hydrogen peroxide can pass easily. According to the results, it can be predicted that lysine amino acids have been modified by GABA molecules and amide bond formed between them.

Fig. 14

Fig.15

4. Conclusion

In summary, immobilization of HRP onto the MWCNT-COOH-GABA composite was accomplished by covalent bonding between the carboxyl group of GABA and amine groups of amino acids of HRP. Due to the compatibility of GABA, covalent attachment of enzyme the biosensor also exhibits high stability, reproducibility and repeatability. The MWCNT-COOH-GABA decreases resistance and increases electron transfer at the electrode surface and hence an increase in current response. The newly constructed biosensor demonstrated excellent electrocatalytic activity towards the reduction of H_2O_2 in PBS (pH=7) solution. The surface coverage of HRP on the surface of the modified electrode and the apparent Michaelis–Menten constant were calculated to be 3.029×10^{-9} mol cm^{-2} and 0.23 mM, respectively. The electron transfer rate constant of the biosensor was obtained 1.11 s^{-1}. This novel biosensor displayed low

detection limit (0.13 μM) and large linear range 0.2 to 281 μM for H_2O_2. Based on comfortable preparation, great properties and low detection limit, the biosensor could use particularly for H_2O_2 determination in a real sample like human plasma. In molecular docking calculations, it was shown that GABA molecules tend to lysine amino acids of HRP and so these residues can be modified by GABA. Molecular dynamics calculations represented that RMSD of the enzyme decreases with the presence of GABA molecules, and thus HRP+GABA moves less than HRP. Also GABA molecules open the pathway for the H_2O_2 to the heme prostatic group and it is therefore suitable for HRP immobilization. The results of the experimental and computational sections confirm each other and are in agreement.

Acknowledgment

We would like to thank the Damghan University for its financial support.

References

[1] S.J. Neill, R. Desikan, A. Clarke, R.D. Hurst, J.T. Hancock, Hydrogen peroxide and nitric oxide as signalling molecules in plants, J. Exp. Bot. 53 (2002) 1237-1247.

[2] C. Chen, X. Hong, T. Xu, A. Chen, L. Lu, Y. Gao, Electrocatalytic oxidation and determination of hydrogen peroxide at poly (N-methylthionine) electrodes, J. Electrochem. Soc. 162 (2015) 699-702.

[3] C. Chen, C. Sun, Y. Gao, Amperometric sensor for hydrogen peroxide based on poly (aniline-co-p-aminophenol), Electrochem. Commun. 11 (2009) 450-453.

[4] P. D'Orazio, Biosensors in clinical chemistry, Clin. Chim. Acta. 334 (2003) 41-69.

[5] R. Stolarek, P. Bialasiewicz, M. Krol, D. Nowak, Breath analysis of hydrogen peroxide as a diagnostic tool, Clin. Chim. Acta. 411 (2010) 1849-1861.

[6] K.M. Mullaugh, R.J. Kieber, J.D. Willey, G.B. Avery Jr, Long-term temporal variability in hydrogen peroxide concentrations in Wilmington, North Carolina USA rainwater, Environ. Sci. Technol. 45 (2011) 9538-9542.

[7] H. Du, X. Guo, R.-M. Kong, F. Qu, Cr_2O_3 nanofiber: a high-performance electrocatalyst toward artificial N 2 fixation to NH_3 under ambient conditions, Chem.Comm. 54 (2018) 12848-12851.

[8] H. Du, R.-M. Kong, X. Guo, F. Qu, J. Li, Recent progress in transition metal phosphides with enhanced electrocatalysis for hydrogen evolution, Nanoscale, 10 (2018) 21617-21624.

[9] A. Kafi, M. Naqshabandi, M.M. Yusoff, M.J. Crossley, Improved peroxide biosensor based on Horseradish Peroxidase/Carbon Nanotube on a thiol-modified gold electrode, Enzyme Microb. Technol. 113 (2018) 67-74.

[10] K. Zhang, L. Mao, R. Cai, Stopped-flow spectrophotometric determination of hydrogen peroxide with hemoglobin as catalyst, Talanta, 51 (2000) 179-186.

[11] M. Magro, D. Baratella, N. Pianca, A. Toninello, S. Grancara, R. Zboril, F. Vianello, Electrochemical determination of hydrogen peroxide production by isolated mitochondria: A novel nanocomposite carbon–maghemite nanoparticle electrode, Sens. Actuator, B: Chem. 176 (2013) 315-322.

[12] F.W. Krainer, A. Glieder, An updated view on horseradish peroxidases: recombinant production and biotechnological applications, Appl. Microbiol. Biotechnol. 99 (2015) 1611-1625.

[13] R.A. Marcus, Electron transfer reactions in chemistry. Theory and experiment, Rev. Mod. Phys. 65 (1993) 599-610.

[14] A. Boujakhrout, P. Diez, A. Sanchez, P. Martinez-Ruiz, J.M. Pingarron, R. Villalonga, Gold nanoparticles-decorated silver-bipyridine nanobelts for the construction of mediatorless hydrogen peroxide biosensor, J. Colloid Interface Sci. 482 (2016) 105-111.

[15] K. Gabrovska, J. Ivanov, I. Vasileva, N. Dimova, T. Godjevargova, Immobilization of urease on nanostructured polymer membrane and preparation of urea amperometric biosensor, Int. J. Biol. Macromol. 48 (2011) 620-626.

[16] M. Rahimi-Mohseni, J.B. Raoof, R. Ojani, T.A. Aghajanzadeh, A.B. Hashkavayi, Development of a new paper based nano-biosensor using the co-catalytic effect of tyrosinase from banana peel tissue (Musa Cavendish) and functionalized silica nanoparticles for voltammetric determination of l-tyrosine, Int. J. Biol. Macromol. 113 (2018) 648-654.

[17] X. Liu, H. Feng, J. Zhang, R. Zhao, X. Liu, D.K. Wong, Hydrogen peroxide detection at a horseradish peroxidase biosensor with a Au nanoparticle–dotted titanate nanotube/hydrophobic ionic liquid scaffold, Biosens. Bioelectron. 32 (2012) 188-194.

[18] M. Baghayeri, E.N. Zare, M.M. Lakouraj, A simple hydrogen peroxide biosensor based on a novel electro-magnetic poly (p-phenylenediamine)@Fe_3O_4 nanocomposite, Biosens. Bioelectron. 55(2014) 259-65.

[19] M. Guler, V. Turkoglu, A. Kivrak, A novel glucose oxidase biosensor based on poly ([2, 2′; 5′,2″]-terthiophene-3′-carbaldehyde) modified electrode, Int. J. Biol. Macromol. 79 (2015) 262-268.

[20] S. Alim, A. Kafi, J. Rajan, M.M. Yusoff, Application of polymerized multiporous nanofiber of SnO2 for designing a bienzyme glucose biosensor based on HRP/GOx, Int. J. Biol. Macromol. 123 (2019) 1028-1034.

[21] Y. Liu, N. Song, Z. Ma, K. Zhou, Z. Gan, Y. Gao, S. Tang, C. Chen, Synthesis of a poly (N-methylthionine)/reduced graphene oxide nanocomposite for the detection of hydroquinone, Mater. Chem. Phys. 223 (2019) 548-556.

[22] M. Eguílaz, R. Villalonga, J. Pingarron, N.F. Ferreyra, G.A. Rivas, Functionalization of bamboo-like carbon nanotubes with 3-mercaptophenylboronic acid-modified gold nanoparticles for the development of a hybrid glucose enzyme electrochemical biosensor, Sens. Actuators, B: chem. 216 (2015) 629-637.

[23] J. Du, L. Ma, D. Shan, Y. Fan, L. Zhang, L. Wang, X. Lu, An electrochemical sensor based on the three-dimensional functionalized graphene for simultaneous determination of hydroquinone and catechol, J. Electroanal. Chem. 722 (2014) 38-45.

[24] N. Li, T. Lv, Y. Yao, H. Li, K. Liu, T. Chen, Compact graphene/MoS 2 composite films for highly flexible and stretchable all-solid-state supercapacitors, J. Mater. Chem. A, 5 (2017) 3267-3273.

[25] Q. Sheng, M. Wang, J. Zheng, A novel hydrogen peroxide biosensor based on enzymatically induced deposition of polyaniline on the functionalized graphene-carbon nanotube hybrid materials, Sens. Actuator, B: Chem. 160 (2011) 1070-1077.

[26] H. Faridnouri, H. Ghourchian, S. Hashemnia, Direct electron transfer enhancement of covalently bound tyrosinase to glassy carbon via Woodward's reagent K, Bioelectrochemistry, 82 (2011) 1-9.

[27] D.S. Jeykumari, S.S. Narayanan, A novel nanobiocomposite based glucose biosensor using neutral red functionalized carbon nanotubes, Biosens. Bioelectron. 23 (2008) 1404-1411.

[28] B. Zhang, J. Zhou, S. Li, X. Zhang, D. Huang, Y. He, M. Wang, G. Yang, Y. Shen, Hydrogen peroxide biosensor based on microperoxidase-11 immobilized on flexible MWCNTs-BC nanocomposite film, Talanta, 131 (2015) 243-248.

[29] J. Huang, W. Zhuang, L. Ge, K. Wang, Z. Wang, H. Niu, J. Wu, C. Zhu, Y. Chen, H. Ying, Improving biocatalytic microenvironment with biocompatible ε-Poly-L-lysine for one step gluconic acid production in low pH enzymatic systems, Process Biochem. 76 (2018) 118-127.

[30] R. Mohammad, M. Ahmad, L.Y. Heng, Amperometric capsaicin biosensor based on covalent immobilization of horseradish peroxidase (HRP) on acrylic microspheres for chilli hotness determination, Sens. Actuator B: Chem. 241 (2017) 174-181.

[31] A. Kermad, S. Sam, N. Ghellai, K. Khaldi, N. Gabouze, Horseradish peroxidase-modified porous silicon for phenol monitoring, Mater. Sci. Eng., B, 178 (2013) 1159-1164.

[32] A.P. Periasamy, S.W. Ting, S.M. Chen, Amperometric and impedimetric H_2O_2 biosensor based on horseradish peroxidase covalently immobilized at ruthenium oxide nanoparticles modified electrode, Int. J. Electrochem. Sci. 6 (2011) 2688-2709.

[33] O. Niwa, R. Kurita, T. Horiuchi, K. Torimitsu, Small-volume on-line sensor for continuous measurement of γ-aminobutyric acid, Anal. Chem. 70 (1998) 89-93.

[34] M. Frisch, G. Trucks, H. Schlegel, G. Scuseria, M. Robb, J. Cheeseman, J. Montgomery Jr, T. Vreven, K. Kudin, J. Burant, Gaussian 03, revision c. 02; Gaussian, Inc., Wallingford, CT, 4 (2004).

[35] G.M. Morris, D.S. Goodsell, R.S. Halliday, R. Huey, W.E. Hart, R.K. Belew, A.J. Olson, Automated docking using a Lamarckian genetic algorithm and an empirical binding free energy function, J. Comput. Chem. 19 (1998) 1639-1662.

[36] U. Essmann, L. Perera, M.L. Berkowitz, T. Darden, H. Lee, L.G. Pedersen, A smooth particle mesh Ewald method, J. Chem. Phys. 103 (1995) 8577-8593.

[37] S.P. Hirshman, J. Whitson, Steepest-descent moment method for three-dimensional magnetohydrodynamic equilibria, Phys. Fluids. 26 (1983) 3553-3568.

[38] J. Li, S. Dong, The electrochemical study of oxidation-reduction properties of horseradish peroxidase, J. Electroanal. Chem. 431 (1997) 19-22.

[39] E. Laviron, The use of linear potential sweep voltammetry and of ac voltammetry for the study of the surface electrochemical reaction of strongly adsorbed systems and of redox modified electrodes, J. Electroanal. Chem. Interfacial. Electrochem. 100 (1979) 263-270.

[40] S.Q. Liu, H.X. Ju, Renewable reagentless hydrogen peroxide sensor based on direct electron transfer of horseradish peroxidase immobilized on colloidal gold-modified electrode, Anal. Biochem. 307 (2002) 110-116.

[41] E. Laviron, General expression of the linear potential sweep voltammogram in the case of diffusionless electrochemical systems, J. Electroanal. Chem. Interfacial. Electrochem. 101 (1979) 19-28.

[42] Y.T. Kong, M. Boopathi, Y.B. Shim, Direct electrochemistry of horseradish peroxidase bonded on a conducting polymer modified glassy carbon electrode, Biosens. Bioelectron. 19 (2003) 227-232.

[43] P. Raghu, T.M. Reddy, B.K. Swamy, B. Chandrashekar, K. Reddaiah, M. Sreedhar, Development of AChE biosensor for the determination of methyl parathion and monocrotophos in water and fruit samples: a cyclic voltammetric study, J. Electroanal. Chem. 665 (2012) 76-82.

[44] A. Safavi, N. Maleki, E. Farjami, Electrodeposited silver nanoparticles on carbon ionic liquid electrode for electrocatalytic sensing of hydrogen peroxide, Electroanalysis, 21 (2009) 1533-1538.

[45] C. Camacho, J.C. Matías, B. Chico, R. Cao, L. Gomez, B.K. Simpson, R. Villalonga, Amperometric Biosensor for Hydrogen Peroxide, Using Supramolecularly Immobilized Horseradish Peroxidase on the β-Cyclodextrin-Coated Gold Electrode, Electroanalysis, 19 (2007) 2538-2542.

[46] N. Mogharrab, H. Ghourchian, M. Amininasab, Structural stabilization and functional improvement of horseradish peroxidase upon modification of accessible lysines: experiments and simulation, Biophysical journal, 92 (2007) 1192-1203.

[47] C. Kaçar, B. Dalkiran, P.E. Erden, E. Kiliç, An amperometric hydrogen peroxide biosensor based on Co_3O_4 nanoparticles and multiwalled carbon nanotube modified glassy carbon electrode, Appl. Surf. Sci. 311(2014) 139-46.

[48] X. Zheng, Y. Guo, J. Zheng, C. Ma, X. Zhou, J. Lin, et al., A hydrogen peroxide biosensor based on horseradish peroxidase/poly(L-leucine)/polydopamine modified glassy carbon electrode, Russ. J. Electrochem. 53(2017) 443-51.

[49] Y. Yang, M. Yang, H. Wang, J. Jiang, G. Shen, R. Yu, An amperometric horseradish peroxidase inhibition biosensor based on a cysteamine self-assembled monolayer for the determination of sulfides, Sens. Actuators, B: Chem. 102 (2004) 162-168.

[50] C. Chen, X. Hong, T. Xu, A. Chen, L. Lu, Y. Gao, Hydrogen peroxide biosensor based on the immobilization of horseradish peroxidase onto a poly (aniline-co-N-methylthionine) film, Synth. Met. 212 (2016) 123-130.

[51] K. Zhou, Y. Zhu, X. Yang, J. Luo, C. Li, S. Luan, A novel hydrogen peroxide biosensor based on Au–graphene–HRP–chitosan biocomposites, Electrochim. Acta. 55 (2010) 3055-3060.

[52] Y. Xin, X. Fu-bing, L. Hong-wei, W. Feng, C. Di-zhao, W. Zhao-yang, A novel H_2O_2 biosensor based on Fe_3O_4–Au magnetic nanoparticles coated horseradish peroxidase and graphene sheets–Nafion film modified screen-printed carbon electrode, Electrochim. Acta. 109 (2013) 750-755.

Table 1

Comparison of analytical performance of the fabricated H_2O_2 biosensor with previous reported.

Electrode	Detection Limit (μM)	linear range (μM)	K_m^{app} (mM)	References
Co_3O_4/MWCNTs/Gelatin/HRP/GCE	0.74	0.74−190	----	[47]
HRP-Chit/PL-LEU/PDA/GCE	0.1	0.5–952.0	0.12	[48]
HRP–SAM–Au electrode	0.3	0.5–12.7	6.34	[49]
PAN-PNMThH/HRP electrode	3.2	5.0-600	2.79	[50]
Au/GS/HRP/CS	1.7	5.0 to 513	2.61	[51]
Hb–PpPDA@Fe_3O_4/GCE	0.21	0.5–400	0.088	[18]
SPCE|GS–Nafion/Fe_3O_4–Au-HRP	12	20 to 250	----	[52]
MWCNT-COOH-GABA/HRP/GCE	0.13	0.2 to 281	0.23	Present work

Chit: Chitiosan, PL-LEU/PDA: poly (L-leucine)/polydopamine, SAM: self-assembled monolayer, PAN-PNMThH: poly (aniline-co-N-methylthionine.

Table 2

Determination of H_2O_2 in human plasma sample (n=4) at MWCNT-COOH-GABA/HRP/GCE

Sample	Added (μM)	Found (μM)	Recovery	t-test value (t4 = 2.78)	Relative Standard Deviation (RSD)
1	4.15	4.23	102.02	0.99	4.14%
2	8.26	8.15	98.91	0.65	4.06%

Figure Captions

Fig.1. Schematic representation of MWCNT-COOH activation.

Fig. 2. Schematic representation of biosensor fabrication process.

Fig. 3. Structure of GABA.

Fig. 4. FT-IR spectra of (a) MWCNT, (b) MWCNT-COOH, (c) MWCNT-COOH-GABA.

Fig. 5. Scanning electronic micrographs of (A) MWCNT-COOH-GABA/GCE, (B) MWCNT-COOH-GABA/HRP/GCE.

Fig. 6. Nyquist plots of bare GCE, MWCNT-COOH/GCE, MWCNT-COOH-GABA /GCE and MWCNT-COOH-GABA/HRP/GCE in 5.0 mM $K_3Fe(CN)_6/K_4Fe(CN)_6$ with 0.10 M KCl as the supporting electrolyte .AC amplitude: 5mV; frequency range: 0.1–100 Hz.

Fig. 7. Cyclic voltammograms of (a) bare GCE, (b) MWCNT-COOH/GCE, (c) MWCNT-COOH/HRP/GCE, (d) MWCNT-COOH-GABA/GCE and (f) MWCNT-COOH-GABA/HRP/GCE in 10.0 mL 0.1 M pH=7.0 PBS. Scan rate 100 mV s^{-1}

Fig. 8. Typical cyclic voltammograms of MWCNT-COOH-GABA/HRP/GCE and the calibration plot of wave current at different scan rates in PBS pH=7.0 ((a) 20, (b) 40, (c) 60, (d) 80, (e) 100, (f) 150, (g) 200, (h) 250, (i) 300, (j) 350, (k) 400, (l) 450, (m) 500 mV s^{-1}. Inset A: plot of the peak current against the scan rate. Inset B: log I_{pc} vs. log ν.

Fig. 9. Variation of (a) the anodic and (b) cathodic peak potential vs log ν.

Fig. 10. The effect of pH on the redox behavior of MWCNT-COOH-GABA/HRP/GCE in 0.1 M PBS solution at different pH (from 5.0 to 8.5). Inset: plots of formal potential vs. pH.

Fig. 11. (A) Differential pulse voltammograms of 0.2, 4.19, 7.33, 15.15, 26.28, 51.58, 85.84, 124.08, 167.37, 204.51, 248.68, 281.52, 321.36, 365.76, 404.73 (μM) from (a) to (o), for H_2O_2 in 0.1 M PBS (pH=7.0). (B) graph of peak current vs. the concentration of H_2O_2. Inset: Lineweaver–Burk plots for H_2O_2.

Fig. 12. (A) The storage stability of MWCNT-COOH-GABA/HRP/GCE biosensor in 0.1 M PBS (pH=7.0) at a scan rate of 100 mV s^{-1}. (B) The long-term stability of MWCNT-COOH-GABA/HRP/GCE biosensor after ten weeks, (C) The long-term stability of MWCNT-COOH-GABA/HRP/GCE biosensor by measuring its response current to 80.0 μM H_2O_2.

Fig.13. Ball and stick view of GABA molecules in close contact with lysine residues of HRP enzyme.

Fig.14. (A) Comparison of RMSD of the enzyme in the absence and presence of GABA molecules, (B) solvent accessible surface area of HRP in 30 ns time interval in the absence and presence of of GABA molecules.

Fig. 15. Structural features of the heme crevice in 1ATJ (A) in HRP and (B) in HRP+GABA according to their MD average structures.

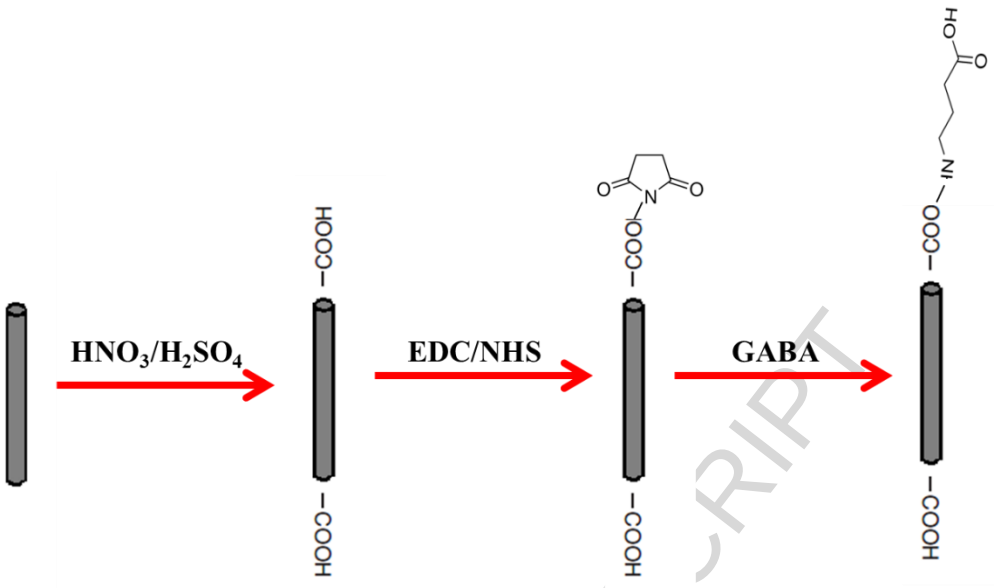

(Figure 1)

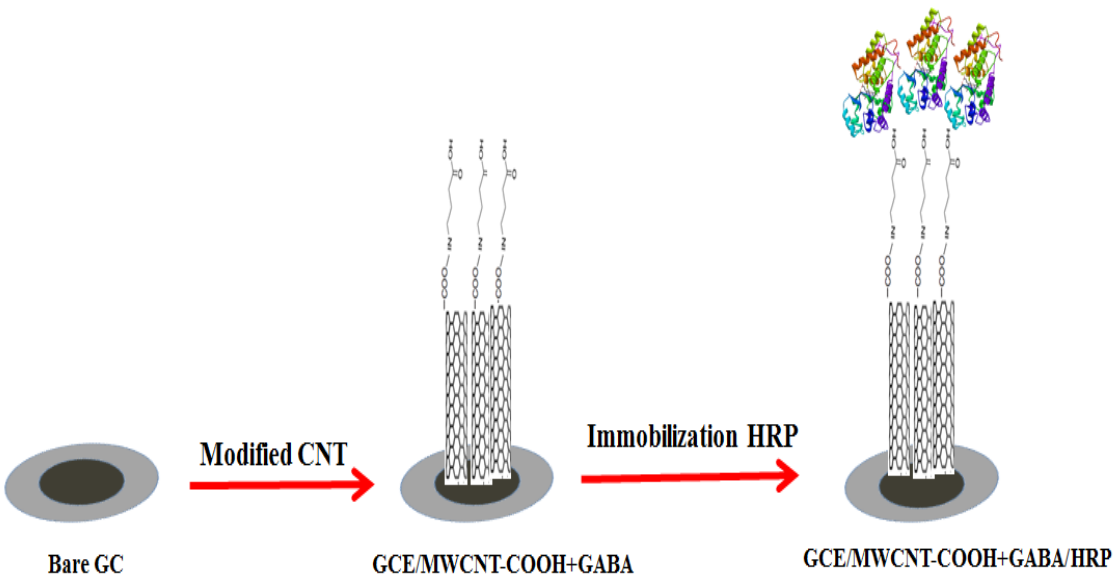

(Figure 2)

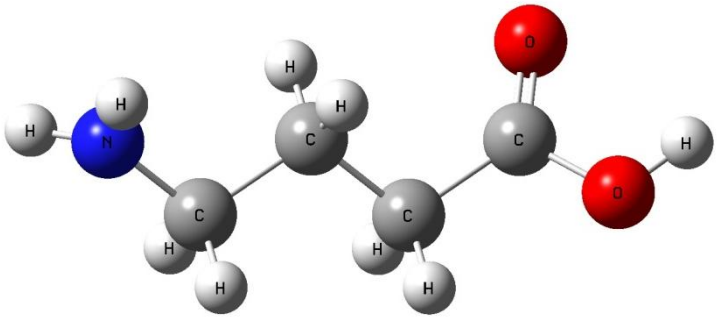

(Figure 3)

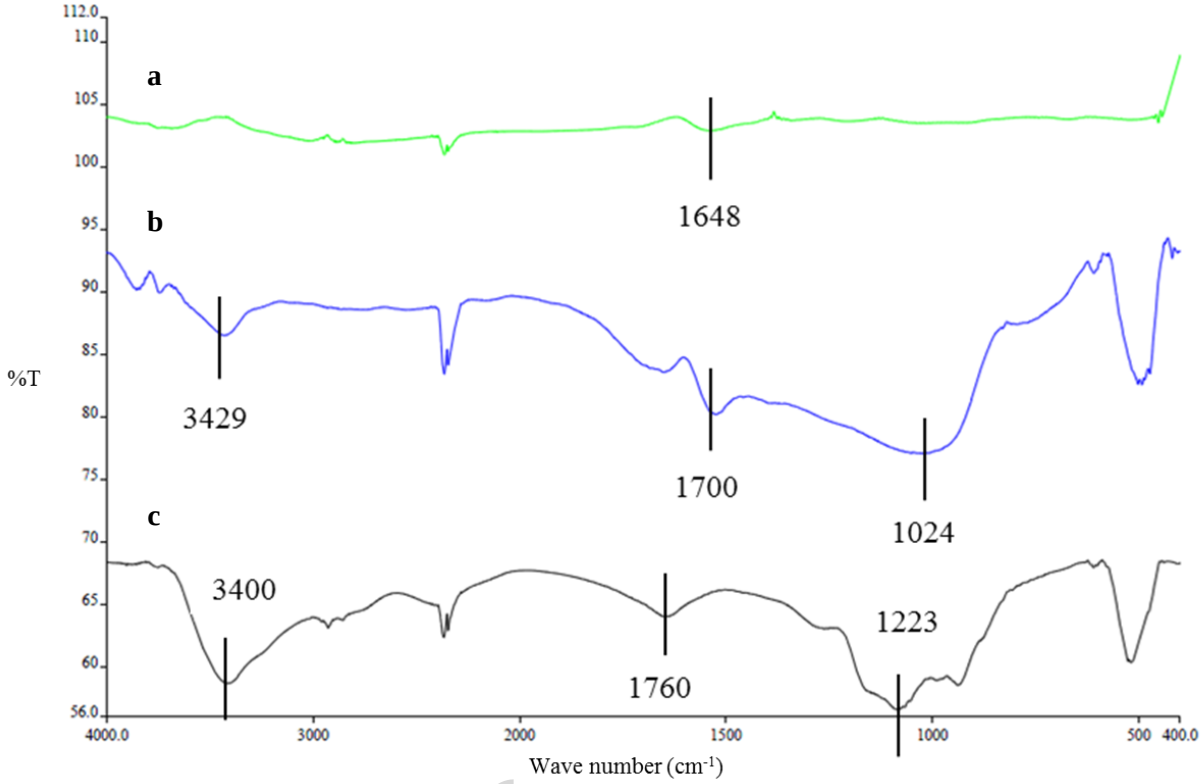

(Figure 4)

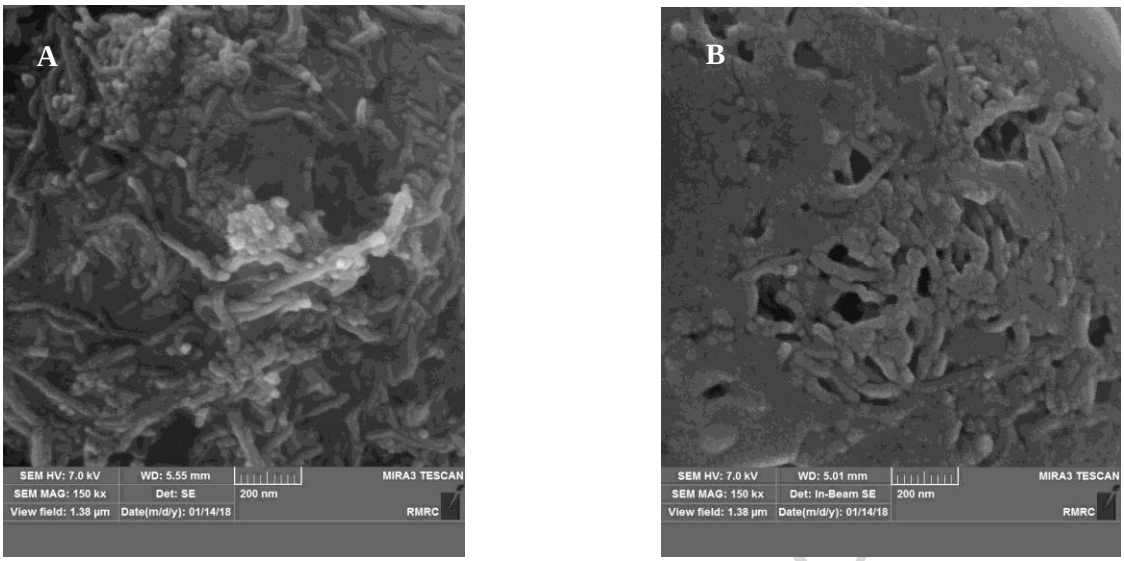

(Figure 5)

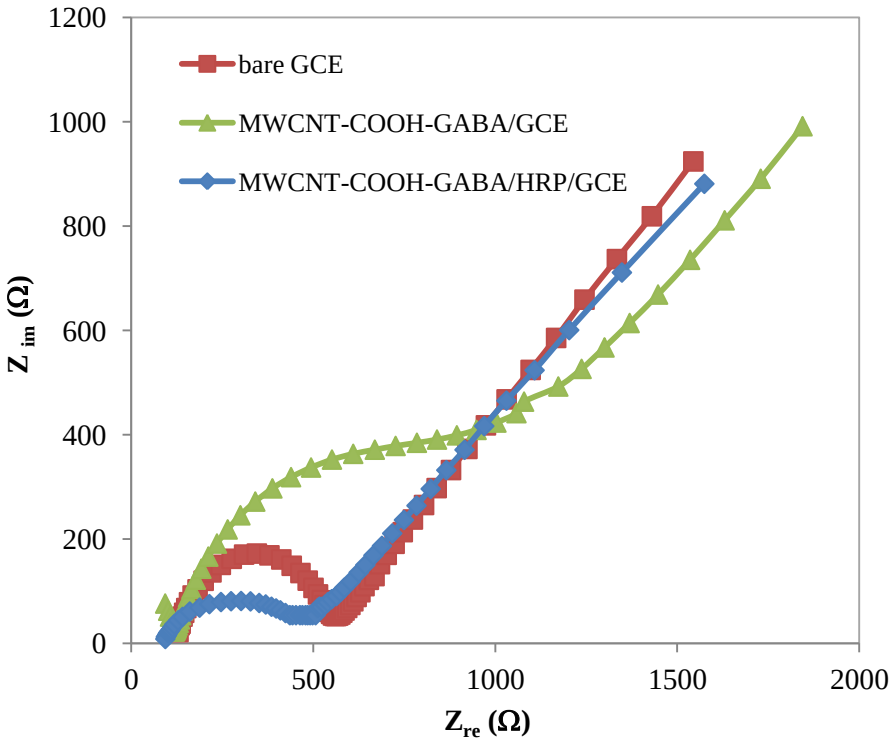

(Figure 6)

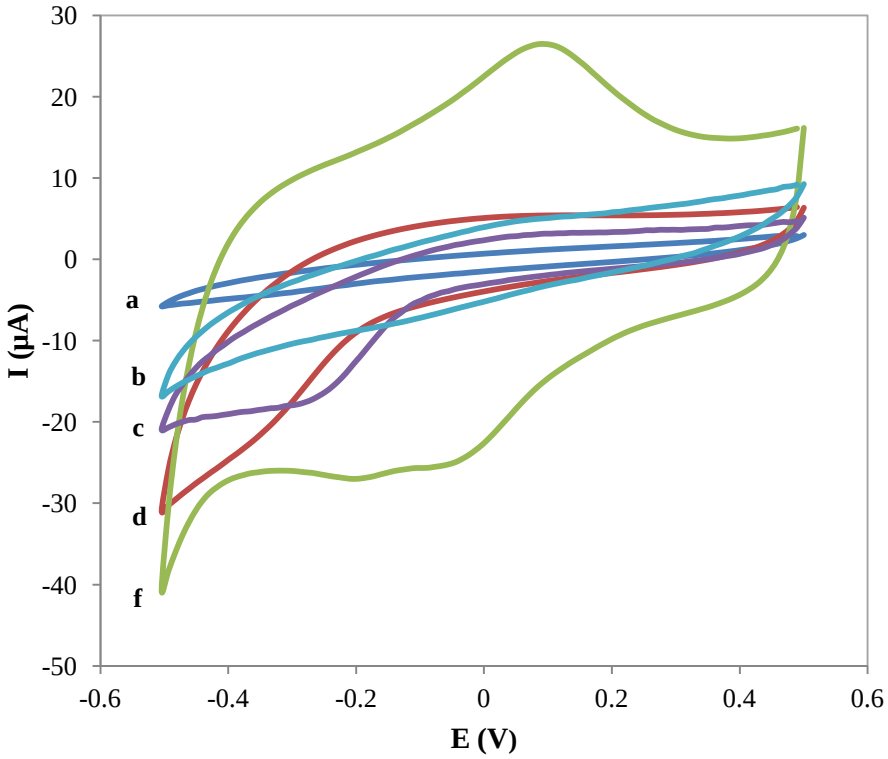

(Figure 7)

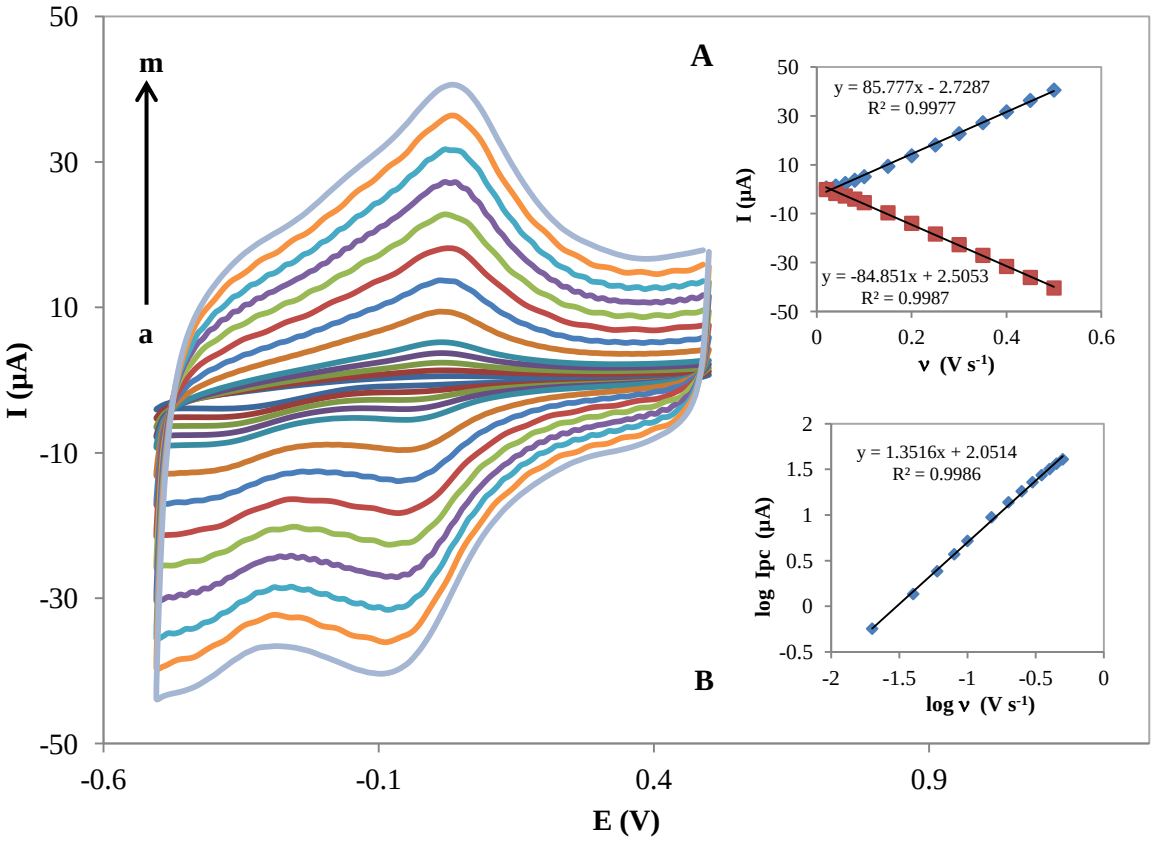

(Figure 8)

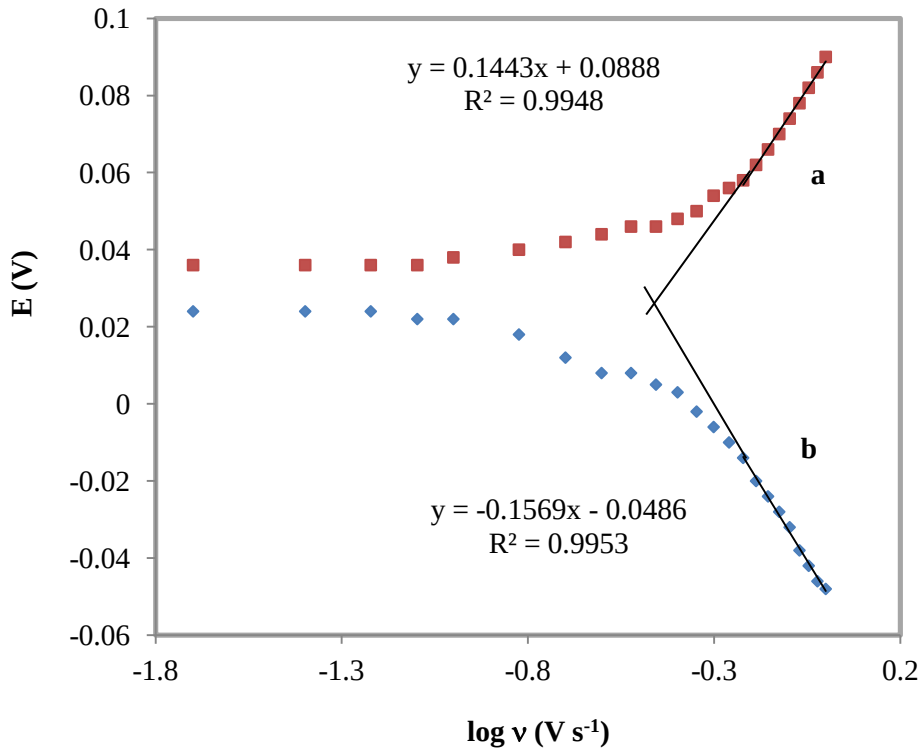

(Figure 9)

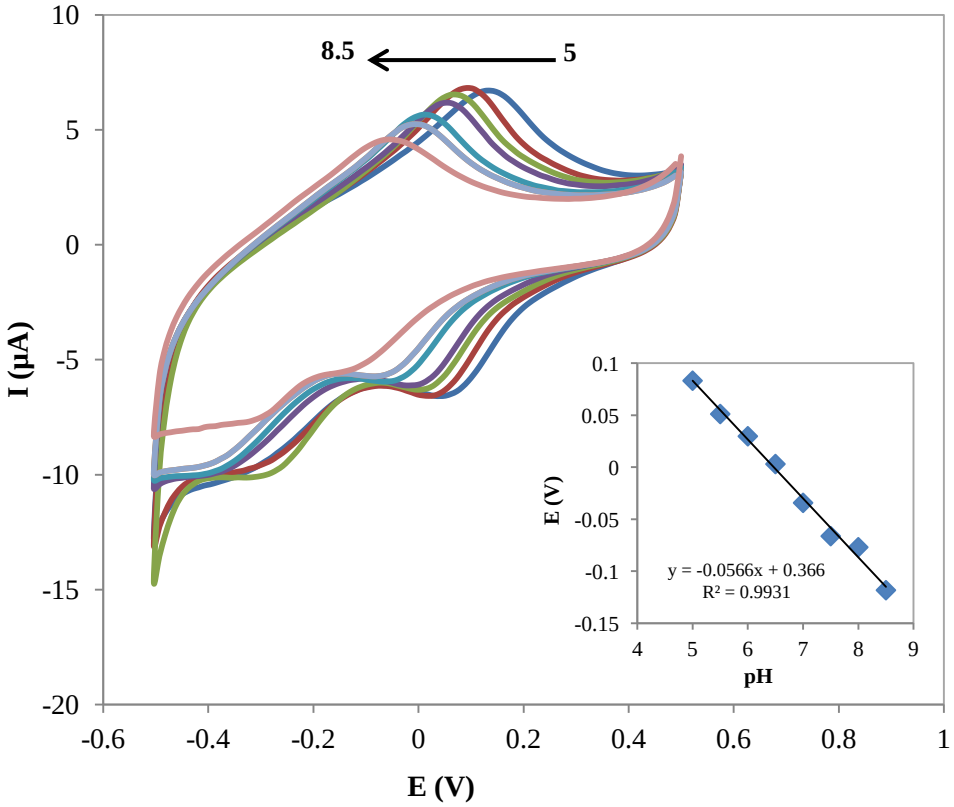

(Figure 10)

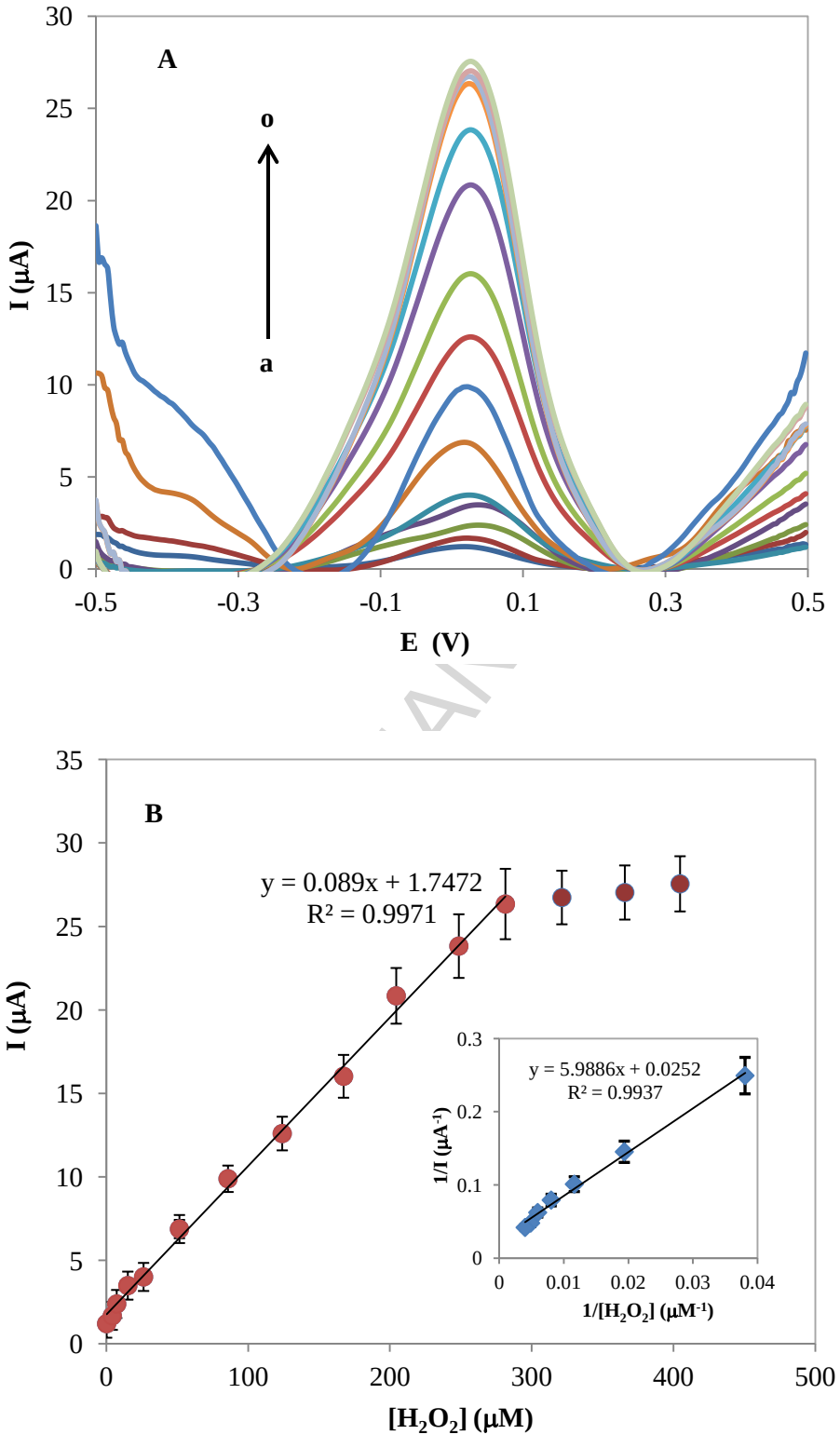

(Figure 11)

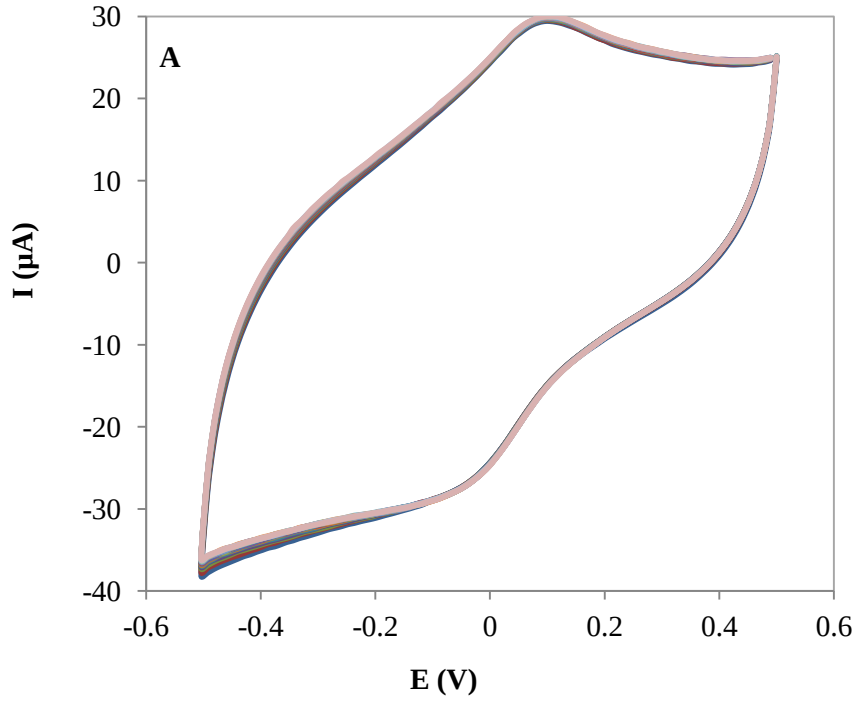

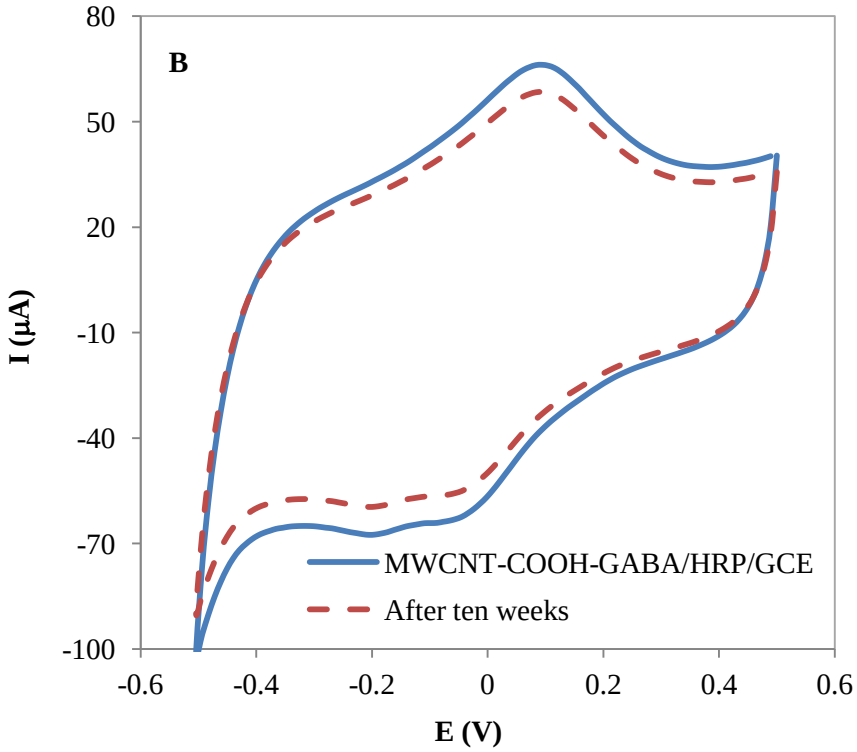

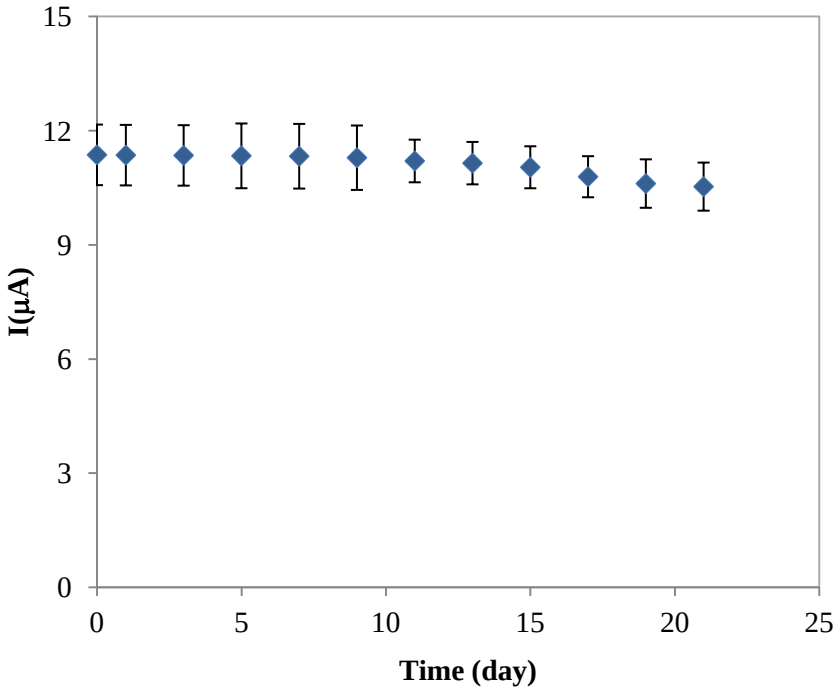

(Figure 12)

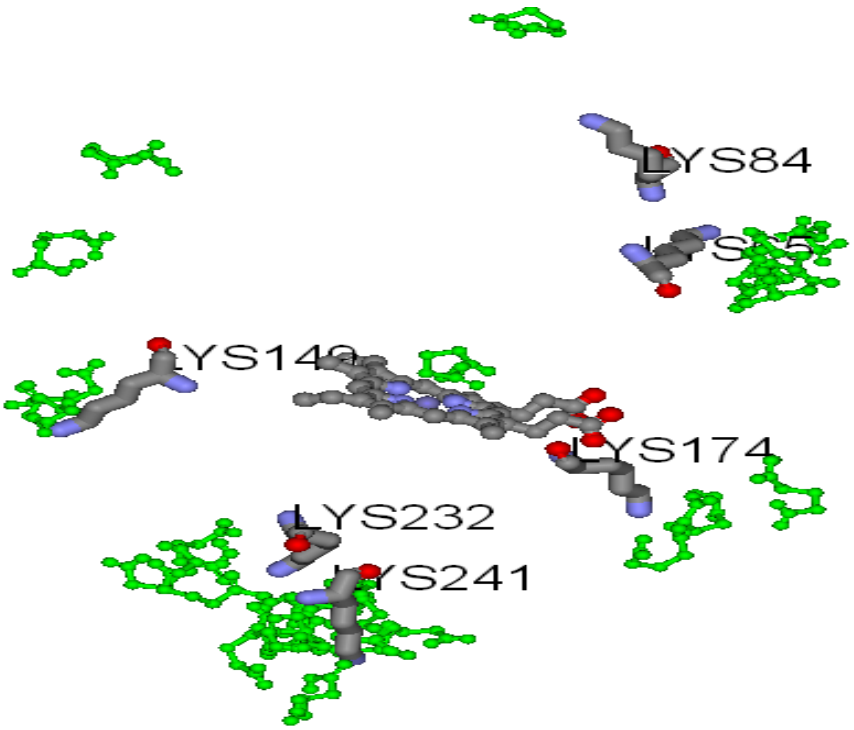

(Figure 13)

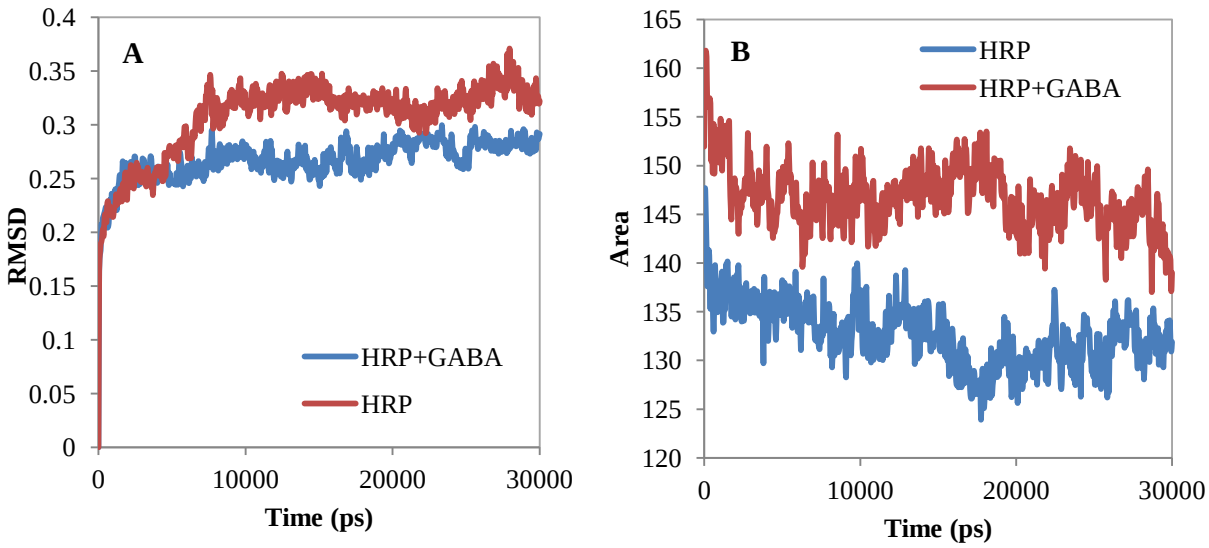

(Figure 14)

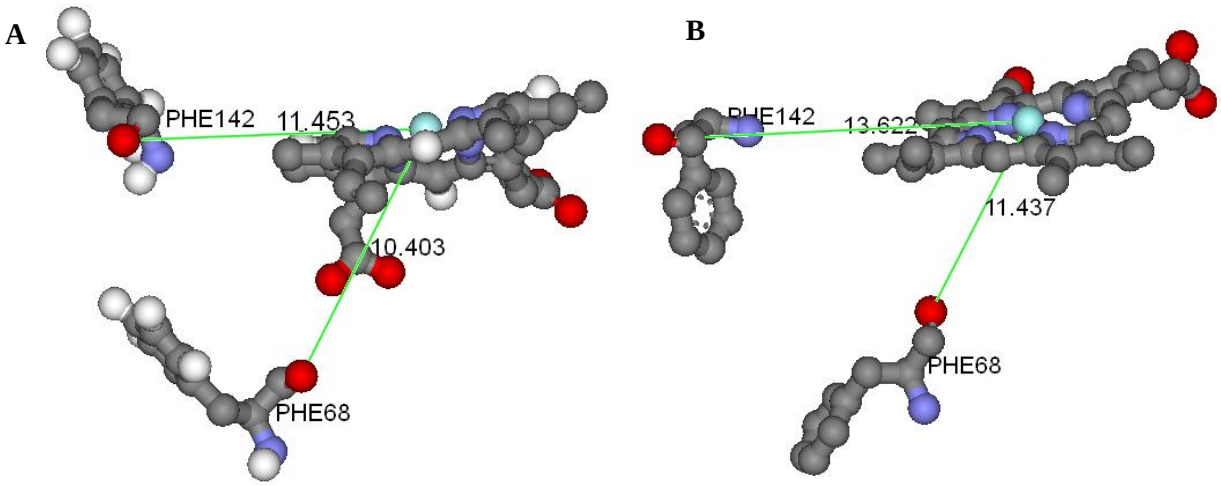

(Figure 15)